



DESIGN AND IMPLEMENTATION OF PREDICTIVE CONTROLLERS ON THE RECTIFIER AND QUASI IMPEDANCE-SOURCE INVERTER IN A WIND ENERGY CONVERSION SYSTEM BASED ON PERMANENT MAGNET SYNCHRONOUS GENERATOR

Hamed Javaheri Fard

Faculty of Engineering

SHAHED University

Iran, Tehran

Email: Javaheri1986@rocketmail.com,+989194598486

Submitted: Nov. 14, 2016

Accepted: Apr. 23, 2017

Published: June 1, 2017

Abstract - Two controllers are proposed in this paper. These controllers have been designed and implemented on the rectifier and quasi impedance-source inverter (QZSI) in the wind energy conversion system based on permanent magnet synchronous generator (PMSG). Model based predictive control strategy (MBPC) has been used at the proposed design for both controllers. Control of parameters such as load current, inductor current and capacitor voltage are the major aim of design of predictive controllers; hence; two cost function (CF) are employed to realize this subject which in those exist objective controls. The MATLAB-simulation and experimental results show that the predictive controllers can be robust and effective in controlling the desired parameters.

Index terms: Predictive Control, Wind Energy, Permanent Magnet Synchronous Generator, Rectifier, Quasi Impedance-Source Inverter.

I. INTRODUCTION

The energy requirements of world have considerably increased according to the recorded statistics in the past 30 years. The International Energy Agency (IEA) forecast of 2014 indicates a 37% energy demand increase in the next 25 years primarily coming from emerging economies in Asia, Africa, Latin America, and the Middle East [1]. In recent years, the use of renewable energy is taken into consideration in order to electric power generation. These energy resources have many advantages relative to other resources (such as fossil energy sources). Renewable energy is one of the most remarkable subjects at the present time due to the high pollution generated from classical energy sources [2].

The wind energy is one of the energy resources which used more than any other renewable energy sources. For the reason its high energy generation potential and minimal environmental impact, wind energy is a comprehensive solution to the growing global energy demand [3]. The wind is a neat, free and endless energy source. It becomes the third core energy resource following non-conventional fuels as oil and chemical [4]. Electrical energy produced by wind power plants is the swiftest developing and most hopefulness renewable energy source [4].

Wind turbines are categorized into two kinds in the wind energy conversion system namely fixed speed and variable speed. The variable speed type produces the most energy in comparison with the fixed speed type. Also, the variable speed type decrease power fluctuations and ameliorate reactive power supply.

Various structures of generators and power electronic circuits that can be used in the wind energy conversion system are shown in Fig.1 and Fig.2, respectively. In the wind power generation systems, generators can be classified into four primary types: I) fixed-speed squirrel-cage induction generator [5,6], II) variable-speed wound rotor induction generator [7] that applies variable rotor resistance, III) variable-speed doubly fed induction generator (DFIG) [8,9] that applies a frequency converter between the grid and its rotor windings and IV) variable-speed synchronous generator [10], which is either a wound rotor synchronous generator or a permanent-magnet synchronous generator (PMSG). Depending on the specific structure is used, the term of power converter in the two figures includes different types of power electronics components such as a soft starter (a), an external-variable resistor for the rotor (c), a rectifier connected to the stator (e) and or connected to the rotor (f, g, h) and or a frequency converter (b, d, e, g, h). In fact,

generators and power electronic converters are two main elements in the structure of a wind energy conversion system.

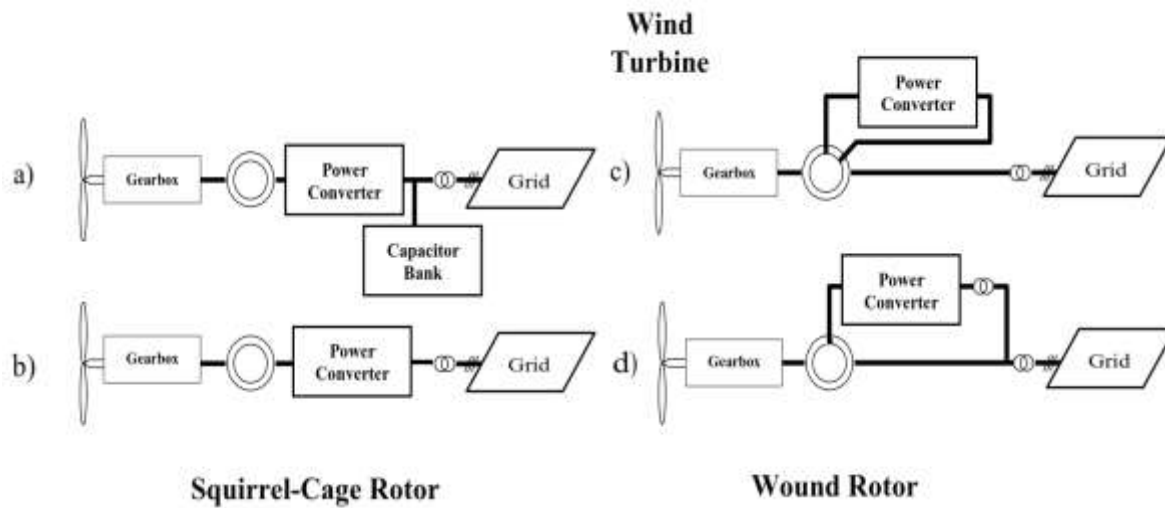


Figure.1. Standard structures of wind turbine using Induction Generator

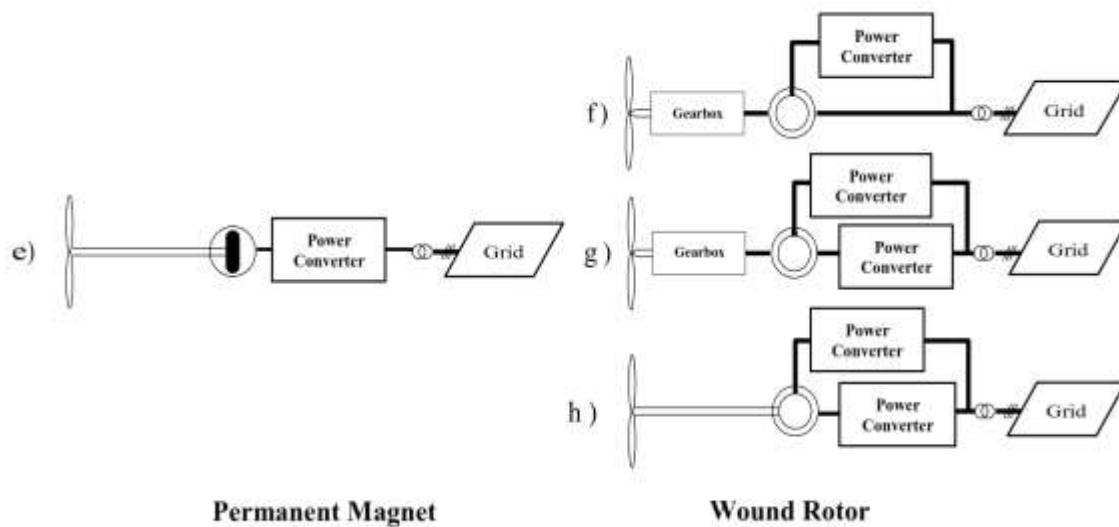


Figure.2. Standard structures of wind turbine using Synchronous Generator

A variety of generator technologies and power electronics topologies for wind turbines is completely shown in [11-14].

In parallel with the development of wind energy conversion systems structure, issues associated with modeling and control their electrical elements are in progress; too. For example in [15] modeling of independent control PMSG wind turbine is done. Two voltage source inverters are applied to control wind turbine linking with the grid because of well independent control; Due to the presence of the two converters will be faced with increasing costs. In [16] an adaptive control technique with the fuzzy method is applied to speed control. Although, this strategy gains the highest power for a specified wind velocity but mathematical calculations will be even more. The sliding mode control strategy has been used in [17]. There is the same previous problem due to a fuzzy-neural network; in addition, there will also be chattering phenomenon. In [18] control of matrix converter has been investigated in the wind turbine based on DFIG; here, the main problem is the matrix converters commutation. In [19] predictive control strategy has been implemented on three-level NPC power converter in wind turbine systems based on PMSG. Although, the employed strategy is very advanced it should be noted that the main problem is the DC link capacitor voltage unbalance.

Therefore, from all these examples can be found that using the best control strategies in the structure of wind energy conversion system is certainly necessary.

Various control techniques have been proposed in the scientific works for the control of the back-to-back power converter used to link the PMSG to the electrical grid; for example, Direct Torque Control (DTC) [20], and Direct Power Control (DPC) [21].

This paper uses the model based predictive control strategy in order to control the parameters of rectifier and quasi impedance-source inverter (QZSI) in a wind energy conversion system based on permanent magnet synchronous generator. So far, the design and simulation and implementation of these kinds of controllers (predictive controller) along by power converter like quasi impedance-source inverter (QZSI) in the mentioned application have not been performed. This research paper is organized as follows; in section II, the total system under study has been presented. Then, section III shows mathematics model of wind turbine. Also, section IV discusses about mathematic model of PMSG. Section V presents MBPC principle. Sections VI and VII present proposed MBPC on the rectifier and proposed MBPC on the QZSI, respectively. Finally, simulation results in section VIII and experimental results in section IX are given.

II. Wind Energy Conversion System under Study

The proposed structure of the wind power generation system is shown in Fig.3. In the present study, at first wind energy is received by the turbine; then, it is converted by the PMSG and finally transferred to the load through a three-phase PWM rectifier in series with QZSI.

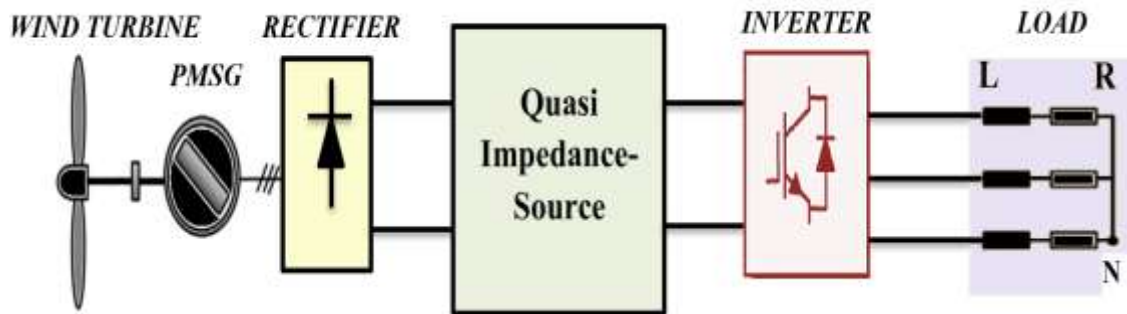


Figure.3. Proposed wind generation system based on PMSG with QZSI

Generally, in standard wind power generation systems are employed different kinds of power electronic converters for various aims, rectifier in order to rectify the generator output, boost converter to enhance the output of the rectifier before feeding the inverter as the output of the inverter is evermore fewer than the input voltage and eventually the inverter to convert the dc / ac preparing power to the alternative load, in this standard system numerous converters are employed which result in decreased system efficiency and reliability. Moreover, dead time available in among switches of each leg makes distortion in the output waveform [22].

In the proposed structure the principal role of PWM rectifier is to adjust the power factor of the PMSG and in order to warrant sinusoidal generator currents. As well as, QZSI can be used to intensify the general system performance. The QZSI can execute both the boost and inversion action; consequently the boost converter can be deleted [22]. Therefore, total cost is reduced and weight of system as well as is declined.

It seems that usage of PMSG in the structure is the most prosperous configuration because of declined conservation cost, high accuracy, and enhanced reliability of electrical grid due to the lack of gearbox.

III. Physics Model of Wind Turbine

For steady-state calculations mechanical power from a wind turbine, the $C_p(\lambda, \beta)$ curve can be used. Mechanical power can be determined with the following equation,

$$P_{mec} = \frac{1}{2} \rho A_r C_p(\lambda, \beta) \cdot v^3 \quad (1)$$

$$\lambda = \frac{\Omega_r r_r}{\omega} \quad (2)$$

Where, the power coefficient (C_p), the angle of blade (β), the tip speed ratio (λ), the wind speed (v), rotor speed (Ω_r), the radius of the rotor (r_r), the air density (ρ), and the area swept by rotor (A_r).

The power coefficient is defined as follows,

$$C_p = \frac{1}{2} (\lambda - 0.022\beta^2 - 5.6) e^{-0.17\lambda} \quad (3)$$

The air density is 1.225 kg/m^3 at atmospheric pressure. Since the site location is effective in air density, therefore, the following equation is considered,

$$\rho = 1.225 e^{-(0.297/3048)h} \quad (4)$$

Where, 'h' in unit meter is site height.

IV. Mathematic Model of Permanent-Magnet Synchronous Generator (PMSG)

In this section, dynamic equations of PMSG in d&q synchronous reference frame are reviewed; exactly,

$$V_{s-d} = R_s I_{s-d} + \frac{d\varphi_{s-d}}{dt} - \omega_{d-q} \varphi_{s-q} \quad (5)$$

$$V_{s-q} = R_s I_{s-q} + \frac{d\varphi_{s-q}}{dt} + \omega_{d-q} \varphi_{s-d} \quad (6)$$

$$\varphi_{s-d} = L_{s-d} I_{s-d} + \varphi_{r-d} \quad (7)$$

$$\varphi_{s-q} = L_{s-q} I_{s-q} \quad (8)$$

Where, V_{s-d} , V_{s-q} , I_{s-d} , and I_{s-q} are the stator voltage and the stator current in the $d&q$ components, respectively. Also, R_s is the stator resistance; L_{s-d} and L_{s-q} are the $d&q$ stator inductances. φ_{s-d} and φ_{s-q} are the $d&q$ stator flux linkage. φ_{r-d} is the permanent magnet flux linkage. ω_{d-q} is the angular electrical rotor speed.

As well as, relationship between applied torques equations with the PMSG rotor is,

$$T_{el} = \frac{3}{2} (\varphi_{s-d} I_{s-q} + \varphi_{r-d} I_{s-q}) \cdot N_p \quad (9)$$

$$T_{el} - T_{LO} - T_D = J \frac{d\omega}{dt} \quad (10)$$

Where, T_{el} , T_{LO} , T_D are the electromagnetic torque, the load torque and the damping torque, respectively. ' J ' is the inertia. ' ω ' is the rotational speed. ' N_p ' is number of pole pairs.

V. Model Based Predictive Control Strategy Principle

Model based predictive control (MBPC) being common in the recent decades has been played a significant role in the novel control engineering. This type of control contains the extensive range of applications including big industrial and even food industry as well. The phrase, MBPC, does not represent a particular control procedure; it refers to the wide range of the control methods in which obtaining control signal is possible by using minimum of a Cost Function through an explicit processing model [23]. These design methods provides the linear controllers which have the resembling structure and identical degree of freedom [23].

The basic idea emerged in the predictive control family is based on the following cases [23]:

- Applying a model to predict the output of the plant in the future times.
- Calculating a series control with the aid of minimizing of a Cost Function.
- Applying the receding horizon principle which contains the usage of the first control component in the calculated series control at any moment.

Variant algorithms of predictive control strategy between themselves are merely diverse in the model used to show the plant, jamming, and the Cost Function which has to be minimized. This control strategy is frequently applied in the industry. Among the applications of this type of

control are the usages of them in robot arm, steam generators, and so on. These applications indicate the capacity of predictive control strategy to achieve the most effective control systems.

Some of the MBPC benefits are as follows:

- This control strategy can be used to control illimitable fields of processes whether with simple dynamics or with complicated dynamics such as the systems with big time delays, the phase non-minimum systems, or the unstable systems [23].
- The multi-variable systems will be simply controlled by MBPC [23].
- This strategy is appropriate for the dead-time systems [23].

The mentioned strategy also has drawbacks. Obtaining the control signal is more complex than that of the classic Proportional-Integral-Derivative (PID) controllers [23]. If the dynamic of the process does not alter, the controller factors can be prearranged, but all calculations should be repeated for each time sample at the mode of adaptive control. As well as, the mathematical calculations will be more at the presence of constraints. Also, a proper model is an essential necessity. Anyway, the benefits have excellence over disadvantages making it extremely beneficial in the industry.

A. MBPC for Power Converters and Drives

The predictive control contains a widespread category of controllers which has recently been used to control the power converters. With the help of predictive control strategy the cascade structure will be removed, which is generally used for the application of linear control; and this will be a great advantage. Also, one benefit of this strategy is that concepts are much simple and achieved transient responses are extremely fast.

Fig.4 shows prevalent predictive control strategy scheme for power converters and drives. It does not matter what kind of topology is the power converter or how many phases it possesses, however this strategy can be used. The load shown in Fig.4 could be each model of passive and active load, an electrical machine or the electrical grid. In this figure, $X^*(k)$ presented the reference values for predictive control strategy. $X(k)$ represents measured variables that are used in the model to calculate predictions of the controlled variables, namely $X(k+1)$, for each one of 'n' possible switching states that can be voltages, switching states, or currents. The existing error between the predicted and reference values is achieved in order to minimize a cost function and

the switching state; then, switching state that minimizes the cost function is selected. The optimal actuation 'S' is chosen; afterwards, it is applied to the converter.

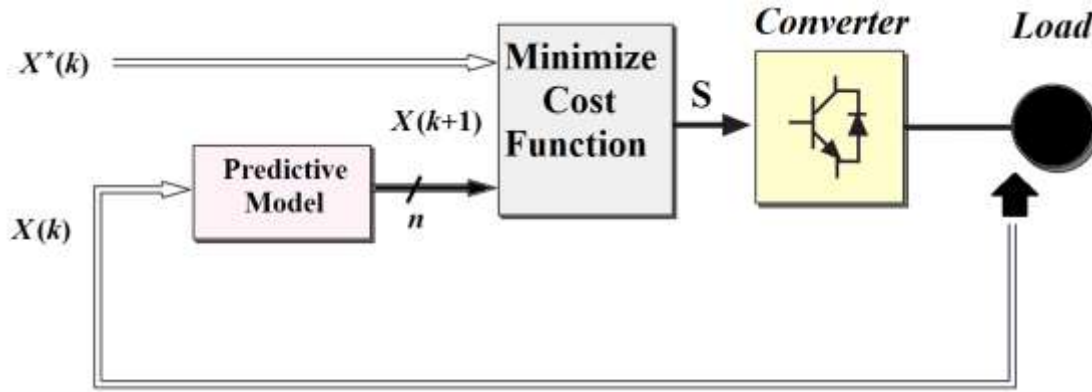


Figure.4. Predictive control strategy block diagram for power converters

VI. Proposed MBPC on the Rectifier Associated with the PMSG

One of the most common power converters, used in energy conversion systems especially wind, is rectifiers. In this section, proposed predictive control strategy is implemented on the converter (rectifier) of the generator side.

To begin, by putting (7) and (8) in (5) and (6), the following equations can be taken. In fact, with the help of stator voltage and stator flux equations, stator current derivatives are extracted in two components d and q .

Thus,

$$\frac{dI_{s-d}}{dt} = (V_{s-d} - R_s I_{s-d} + \omega_{d-q} L_{s-q} I_{s-q}) \left(\frac{1}{L_{s-d}} \right) \quad (11)$$

$$\frac{dI_{s-q}}{dt} = \left\{ V_{s-q} - R_s I_{s-q} + \omega_{d-q} (\phi_{r-d} - L_{s-q} I_{s-d}) \right\} \left(\frac{1}{L_{s-d}} \right) \quad (12)$$

Here, it should be expressed that the stator voltages and currents are in vector state.

The discrete-time model will be employed in order to predict the future value of stator current from voltages and measured currents at the k Th sampling interval. Through this action, implementation of strategy is easier in the simulation software and as well as simulation on digital platforms such as DSP. To achieve a discrete-time model it is requisite to employ some discretization techniques. In here, Stator currents will be discrete in two components with the help of forward Euler discretization method. Thus, the predicted stator current components in $(k+1)$ Th sampling interval are found according to the equations (13) and (14),

$$I_{s-d}(k+1) = \{V_{s-d}(k) - E_{s-d}(k)\} \frac{T_s}{L_{s-d}} + I_{s-d}(k) \left\{ \frac{1 - R_s T_s}{L_{s-d}} \right\} \quad (13)$$

$$I_{s-q}(k+1) = \{V_{s-q}(k) - E_{s-q}(k)\} \frac{T_s}{L_{s-q}} + I_{s-q}(k) \left\{ \frac{1 - R_s T_s}{L_{s-q}} \right\} \quad (14)$$

' T_s ' is the sampling time. In the above equations induced electromotive force (EMF) in two components can be found through the following equations,

$$E_{s-d}(k) = -L_{s-q} \omega_{d-q}(k) I_{s-q}(k) \quad (15)$$

$$E_{s-q}(k) = \omega_{d-q}(k) \{L_{s-d} I_{s-d}(k) + \phi_{r-d}(k)\} \quad (16)$$

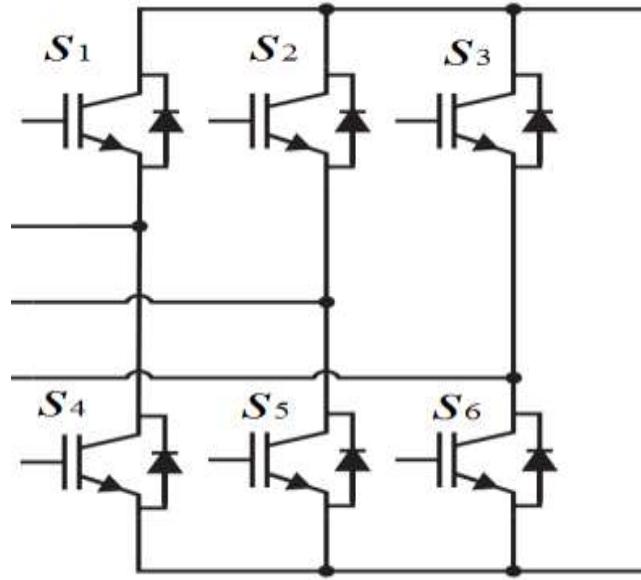


Figure.5. Three-phase rectifier topology

In fact, the proposed MBPC strategy is based on this principle that merely a finite number of possible switching states can be produced by the power converter; also, the operation of the variables is predicted by means certain models of the system in every switching state.

Here, the two switches in each converter of the generator side phase act in a complementary mode due to avoid short circuiting the input voltage (Fig.5). Thus, the number of power switches is six. These switches are considered in the form of three switching signals namely S_A , S_B , S_C , as follows,

$$\begin{aligned} S_A & \left\langle \begin{array}{ll} 1 \Rightarrow & s_1 \rightarrow on \quad s_4 \rightarrow off \\ 0 \Rightarrow & s_1 \rightarrow off \quad s_4 \rightarrow on \end{array} \right\rangle \\ S_B & \left\langle \begin{array}{ll} 1 \Rightarrow & s_2 \rightarrow on \quad s_5 \rightarrow off \\ 0 \Rightarrow & s_2 \rightarrow off \quad s_5 \rightarrow on \end{array} \right\rangle \\ S_C & \left\langle \begin{array}{ll} 1 \Rightarrow & s_3 \rightarrow on \quad s_6 \rightarrow off \\ 0 \Rightarrow & s_3 \rightarrow off \quad s_6 \rightarrow on \end{array} \right\rangle \end{aligned}$$

So, there will be eight switching states according to the following table,

Table 1: Switching states and voltage vectors

S_A	S_B	S_C	Stator Voltage Vectors
0	0	0	$V_0=0$
1	0	0	$V_1=(2/3)V_i$
1	1	0	$V_2=(1/3 +j\sqrt{3}/3) V_i$
0	1	0	$V_3=(-1/3 +j\sqrt{3}/3) V_i$
0	1	1	$V_4=-(2/3)V_i$
0	0	1	$V_5=(-1/3 -j\sqrt{3}/3) V_i$
1	0	1	$V_6=(1/3 -j\sqrt{3}/3) V_i$
1	1	1	$V_7=0$

In table 1, ' V_i ' represents the input voltage; the same voltage at the input quasi impedance-network. It is clear from the table that voltage vectors are composed of two components of real and imaginary; apart from zero and seven vectors that represent a finite set of voltage vectors. If

the real and imaginary parts of the voltage vectors respectively, from zero to seven, $V_{s-\alpha}^N$ and $V_{s-\beta}^N$ designated so that $N=0 \dots 7$ (e.g. $V_1 = (2/3) V_i \rightarrow V_1 = V_{s-\alpha}^1 + 0V_{s-\beta}^1$), the stator voltage vectors in $d&q$ are calculated as follows,

$$V_{s-d}^N(k) = \cos(\theta_{d-q}(k)) \cdot V_{s-\alpha}^N(k) + \sin(\theta_{d-q}(k)) \cdot V_{s-\beta}^N(k) \quad (17)$$

$$V_{s-q}^N(k) = -\sin(\theta_{d-q}(k)) \cdot V_{s-\alpha}^N(k) + \cos(\theta_{d-q}(k)) \cdot V_{s-\beta}^N(k)$$

The relation (17), stator voltage components at the k Th sampling interval, has been attained with the help of a rotating mechanism and using an angle namely ' θ_{d-q} ' in $\alpha&\beta$ frame.

Now, with respect to the voltages in the mentioned evolution, i.e. (17), the stator current vectors in equations (13) and (14) be rewritten as follows,

$$\xrightarrow{N=0 \dots 7} I_{s-d}^N(k+1) = \{V_{s-d}^N(k) - E_{s-d}(k)\} \frac{T_s}{L_{s-d}} + I_{s-d}(k) \left\{ \frac{1 - R_s T_s}{L_{s-d}} \right\} \quad (18)$$

$$\xrightarrow{N=0 \dots 7} I_{s-q}^N(k+1) = \{V_{s-q}^N(k) - E_{s-q}(k)\} \frac{T_s}{L_{s-q}} + I_{s-q}(k) \left\{ \frac{1 - R_s T_s}{L_{s-q}} \right\} \quad (19)$$

In equations (18) and (19), the predicted stator currents have been obtained in $d&q$ reference at the $(k+1)$ Th sampling interval when stator voltage components are applied during k Th sampling interval.

In the following, with the help of reference stator current vectors at the k Th sampling interval, the applied error in the cost function can be found as follows,

$$ErI_{s-d}^N(k+1) = I_{s-d}^*(k) - I_{s-d}^N(k+1) \quad (20)$$

$$ErI_{s-q}^N(k+1) = I_{s-q}^*(k) - I_{s-q}^N(k+1) \quad (21)$$

In relations (20) and (21), symbol of 'Er' represents the error between the reference values and the predicted values. Also, symbol of '*' represents the reference value.

The goal of the control proposed scheme is in order to minimize the occurred error between the measured currents in plant and the reference currents in plant. This necessity can be illustrated in the framework of a cost function. Therefore,

$$CF_1 = |ErI_{s-d}^N(k+1)| + |ErI_{s-q}^N(k+1)| \quad (22)$$

Finally, the switching state which minimizes the cost function is applied to rectifier.

The block diagram of the proposed control scheme can be seen in Fig.6.

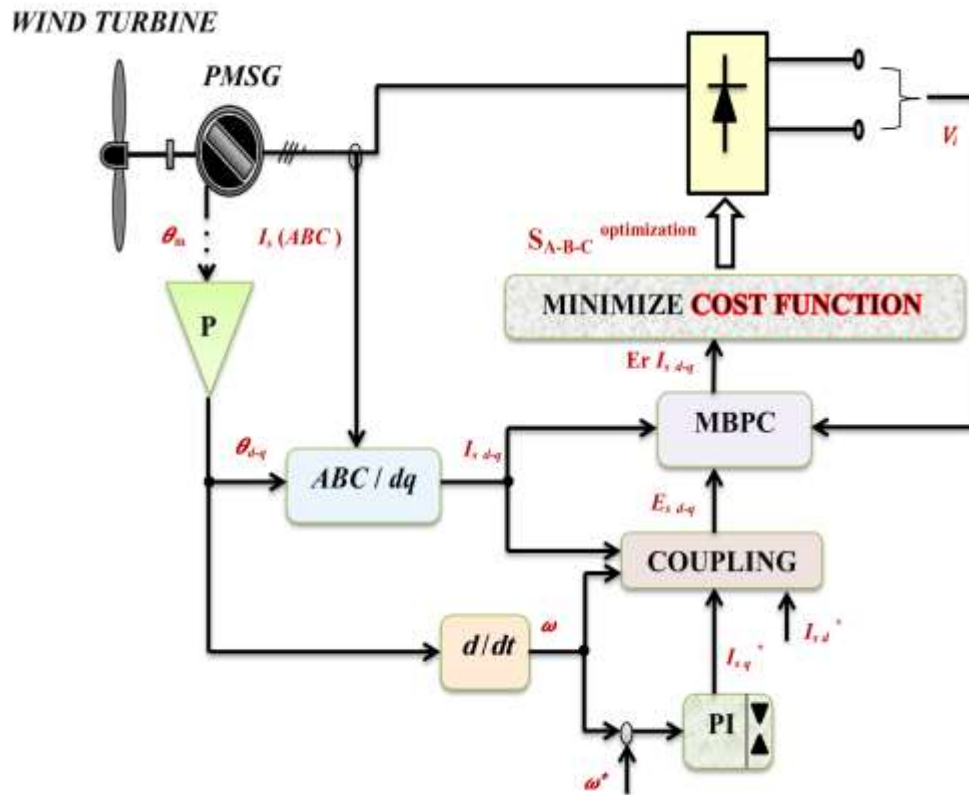


Figure.6. Proposed MBPC for rectifier associated with the PMSG

VII. Proposed MBPC on the QZSI in the Wind Energy Conversion System

A. The Introduction and Function of QZSI

The three-phase Impedance-Source Inverters (ZSI) [24, 25] topology was presented for the first time, with structure of a buck boost inverter in a single stage conversion. It provides a greater voltage boost gain and removes overlapping problem among the inverter switches and a distortion in the inverter output current because of the presence of the dead time. Nevertheless, it has drawbacks of a discontinuous input current and a great voltage stress in between both its capacitors.

An novel and perfected topology of ZSI known as Quasi Impedance-Source Inverter (QZSI) [26, 27] provides a superior option along with the continuous input current and a fewer voltage stress among one of its capacitor while sustaining a same ability as the primary ZSI with the same number of elements.

The structure of a ZSI and a QZSI can be seen in the Fig.7 and Fig.8, respectively.

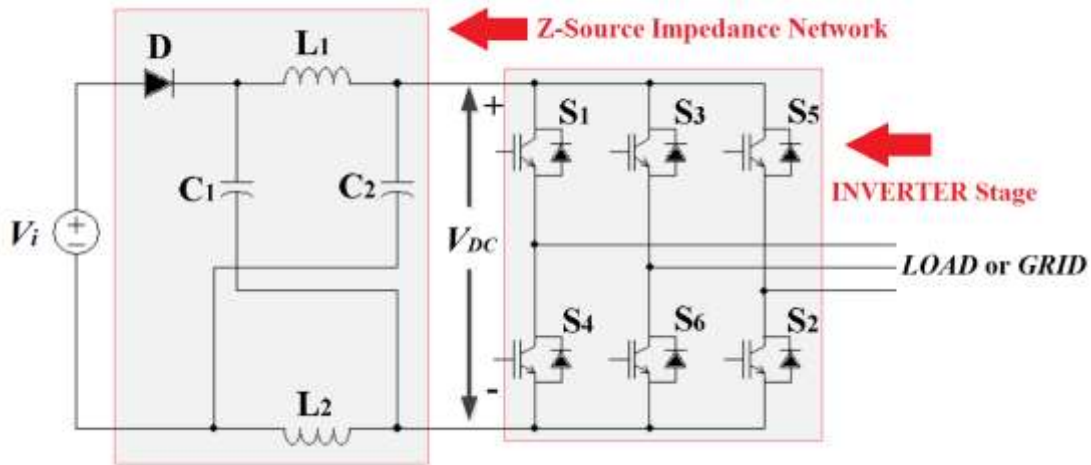


Figure.7. Three-phase Impedance-Source Inverter (ZSI)

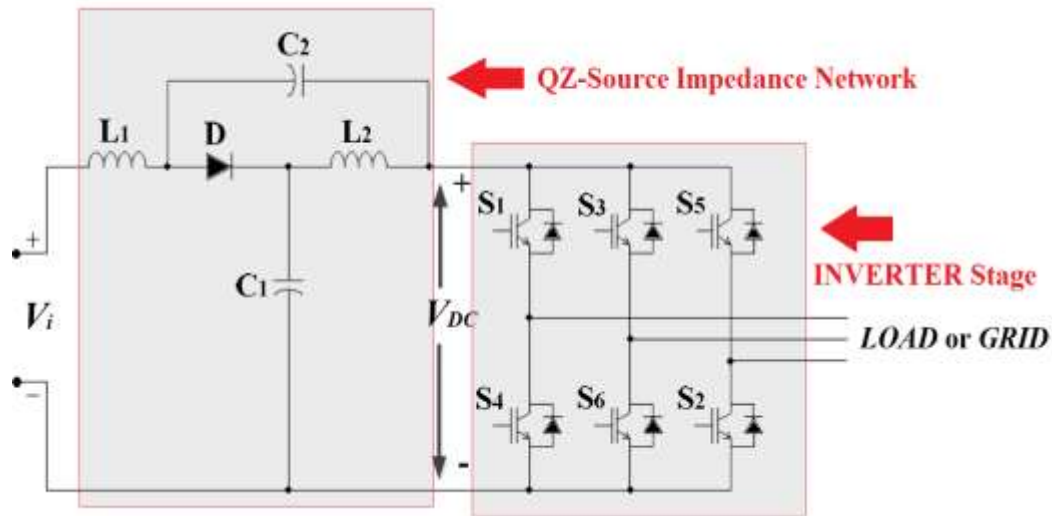


Figure.8. Three-phase Quasi Impedance-Source Inverter (QZSI)

As can be seen in Fig.8, the quasi impedance network has been consist from an asymmetrical 'LC' network including L_1 , L_2 , C_1 , C_2 along with an Diode. The QZSI has three modes of work; these modes are Active state, Null state and Shoot-through state. In the case of active state operation,

inverter will be control similar to typical methods. In the case of null state operation, the upper inverter switches or all of the three under switches of inverter will be switched on. If the two switches are turned on at the same time at a leg, then, the shoot-through state operation will be created; the consequence of this state is that one or three legs of the converter will be short circuit. Consider the Fig.9.

For more information about the QZSI operation modes refer to [27].

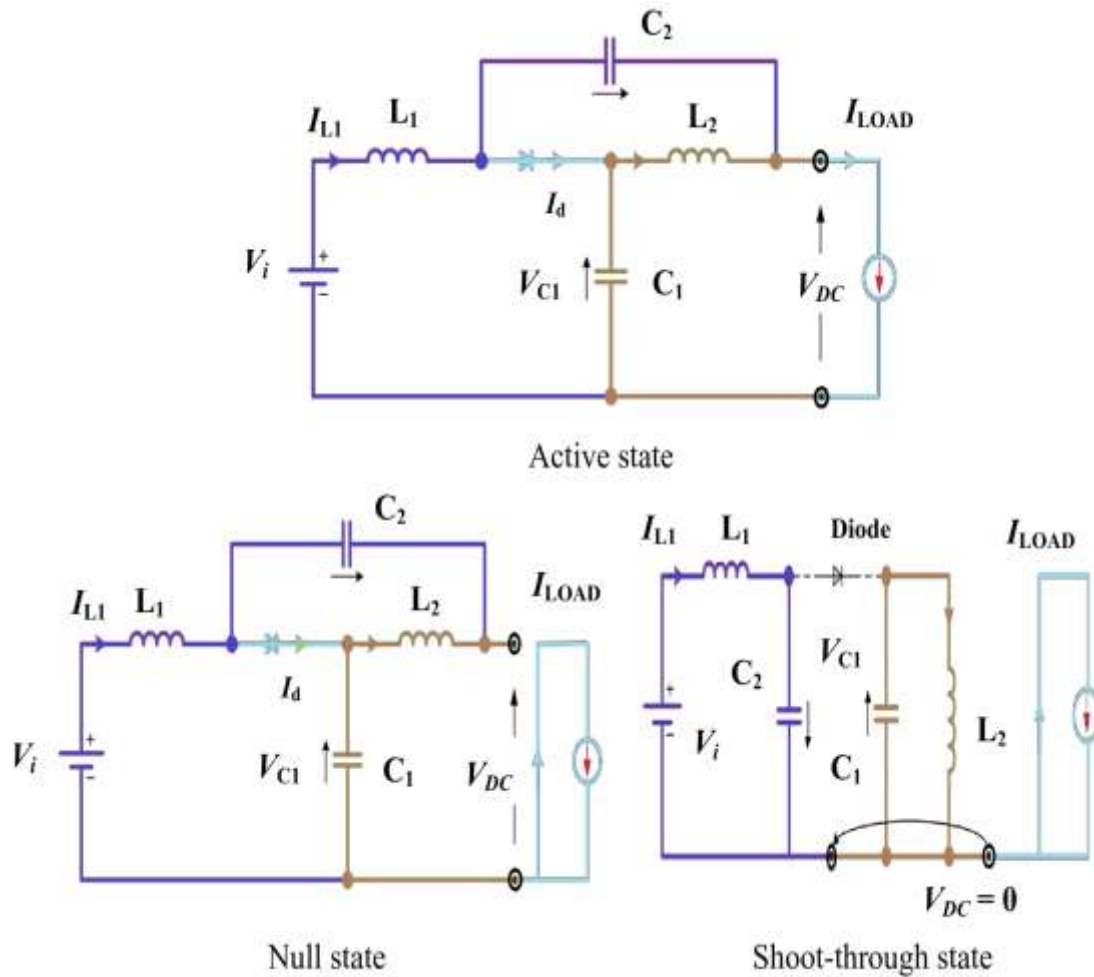


Figure.9. Overall structure of operational modes for QZSI

According to the Fig.8, the basic equations for the QZSI are as follows [27],

$$V_{C1} = \frac{1-d}{1-2d}V_i \quad (23)$$

Where, parameter d is duty ratio and V_{C1} is capacitor voltage C_1 .

$$V_{C2} = \frac{d}{1-2d}V_i \quad (24)$$

$$V_{DC} = \frac{d}{1-2d}V_i \quad (25)$$

Where, V_{C2} is capacitor voltage C_2 and V_{DC} is DC link voltage.

$$d = \frac{T_{SH}}{T} \quad (26)$$

Where, T_{SH} and T are the shoot-through period and the switching period, respectively.

$$B = \frac{1}{1-2d} \quad (27)$$

Where, B is the boost coefficient.

B. Proposed MBPC on the QZSI

The use of the QZSI will cause the entire energy conversion system performance be better compared to the conventional inverters and ZSI. As already was mentioned, the QZSI based system can perform both the boosting and inversion action; accordingly the boost converter can be eliminated [22]. Consequently, the system cost greatly reduces, and weight of system as well decreased. In this section the proposed predictive control strategy is implemented on the QZSI. The overall structure connecting the QZSI to the wind energy conversion system based PMSG is given in the Fig.10.

From the fifteen switching states of inverter, the six states is related to the Active state and the two states is related to the Null state and the remaining, seven, is related to the Shoot-through state; in accordance with the Table 2, [28]. These states are able that be transformed from three-phase to two-phase. It should be expressed that the Null states and the Shoot-through states can be placed in a group since they produce the identical voltage vectors. Therefore, according to this principle, the required time in order to calculate the voltage vectors as well as their number will be reduced.

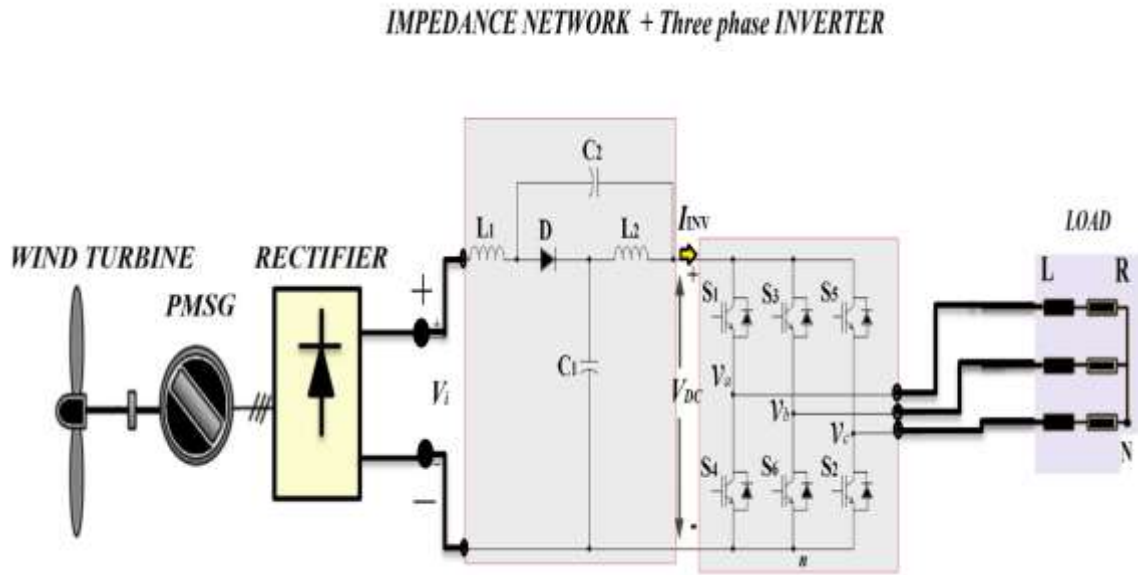


Figure.10. Block diagram-based wind energy conversion system with QZSI topology

Table 2: Switching states and voltage vectors for QZSI

S_1	S_4	S_3	S_6	S_5	S_2	Output Voltage Vectors
1	0	1	0	1	0	$V_0=0$
0	1	0	1	0	1	<i>Null state</i>
1	0	0	1	0	1	$V_1=(2/3)V_{C1}$
1	0	1	0	0	1	$V_2=(1/3 + j\sqrt{3}/3) V_{C1}$
0	1	1	0	0	1	$V_3=(-1/3 + j\sqrt{3}/3) V_{C1}$
0	1	1	0	1	0	$V_4=-(2/3) V_{C1}$
0	1	0	1	1	0	$V_5=(-1/3 - j\sqrt{3}/3) V_{C1}$
1	0	0	1	1	0	$V_6=(1/3 - j\sqrt{3}/3) V_{C1}$
1	1	0	0	0	0	$V_7=0$ <i>Shoot-through state</i>
0	0	1	1	0	0	
0	0	0	0	1	1	
1	1	1	1	0	0	
0	0	1	1	1	1	
1	1	0	0	1	1	
1	1	1	1	1	1	

With regard to the unitary vector namely $a = e^{(j2\pi)/3} = (-1/2) + j(\sqrt{3}/2)$ that indicates the 120 degrees' phase displacement among the phases, the vector of output voltage produced by the inverter can be described as follows,

$$V = \frac{2}{3}(v_{an} + av_{bn} + a^2v_{cn}) \quad (28)$$

According to the Fig.10, v_{an} , v_{bn} , and v_{cn} are the phase to neutral (n) voltages of the inverter.

In accordance with Fig.10, if v_{an} , v_{bn} , and v_{cn} for each phase be defined as follows,

$$v_{an} = L \frac{di_a}{dt} + Ri_a + v_{nN} \quad (29)$$

$$v_{bn} = L \frac{di_b}{dt} + Ri_b + v_{nN} \quad (30)$$

$$v_{cn} = L \frac{di_c}{dt} + Ri_c + v_{nN} \quad (31)$$

Where, R and L are the load resistance and the load inductance, respectively. Moreover, i_a , i_b , and i_c are the current each phase. Note that these currents along with ' v_{nN} ' are not shown on the Fig.10.

Then, through substituting equations (29-31) into (28), this equation can be rewritten as follows,

$$V = L \frac{d}{dt} \left\{ \frac{2}{3}(i_a + ai_b + a^2i_c) \right\} + R \left\{ \frac{2}{3}(i_a + ai_b + a^2i_c) \right\} + \frac{2}{3}(v_{nN} + av_{nN} + a^2v_{nN}) \quad (32)$$

With regard to the vector equation (28) and the following definition for the load current,

$$I_{LOAD} = \frac{2}{3}(i_a + ai_b + a^2i_c) \quad (33)$$

And assuming,

$$\frac{2}{3}(v_{nN} + av_{nN} + a^2v_{nN}) = v_{nN} \frac{2}{3}(1 + a + a^2) = 0 \quad (34)$$

The voltage vector generated by the inverter or the same the output voltage achieves as follows,

$$V = L \frac{dI_{LOAD}}{dt} + RI_{LOAD} \quad (35)$$

In the following, we refer to this important issue that for each of the operation modes, the main variables for prediction action are: the capacitor voltage for C_1 (V_{C1}) that according to the Table

2, output voltage vectors are dependent on it. The inductor current for L_1 (I_{L1}) which it is input current into the quasi impedance network; and finally the load current (I_{LOAD}).

B.i Active State Operation

The following equations are obtained for Active State according to the Fig.9 and as well Fig.10,

$$\frac{dV_{C1}}{dt} = (I_{L1} - I_{INV}) \left(\frac{1}{C_1} \right) \quad (36)$$

$$I_{INV} = I_{LOAD} \rightarrow \text{in Active state}$$

$$\frac{dI_{L1}}{dt} = (V_i - I_{L1}r - V_{C1}) \left(\frac{1}{L_1} \right) \quad (37)$$

Where, ' r ' and I_{INV} are the internal resistance of inductance ' L_1 ' and the input current into the three-phase inverter, respectively.

B.ii Null State Operation

Again from the Fig.9, the equations (38) and (39) will be obtained,

$$\frac{dV_{C1}}{dt} = (I_{L1}) \left(\frac{1}{C_1} \right) \quad (38)$$

$$\frac{dI_{L1}}{dt} = (V_i - I_{L1}r - V_{C1}) \left(\frac{1}{L_1} \right) \quad (39)$$

B.iii Shoot-Through State Operation

Again from the Fig.9, the following equation will be obtained,

$$\frac{dV_{C1}}{dt} = -(I_{L1}) \left(\frac{1}{C_1} \right) \quad (40)$$

$$\frac{dI_{L1}}{dt} = (V_{C1}) \left(\frac{1}{L_1} \right) \quad (41)$$

B.iv Discrete-Time Model for Prediction

Here, the discretization of mentioned variables will be done by a forward Euler approximation.

This discretization is useful in order to predict the future value of capacitor voltage (V_{C1}), the inductor current (I_{L1}), and load current (I_{LOAD}).

Thus, the derivation of mentioned variables will be as follows,

$$\frac{dV_{C1}}{dt} \approx \frac{V_{C1}(t) - V_{C1}(t - T_s)}{T_s} \quad (42)$$

$$\frac{dI_{L1}}{dt} \approx \frac{I_{L1}(t) - I_{L1}(t - T_s)}{T_s} \quad (43)$$

$$\frac{dI_{LOAD}}{dt} \approx \frac{I_{LOAD}(t) - I_{LOAD}(t - T_s)}{T_s} \quad (44)$$

Using the equation (35), the derivative of the load current is extracted as follows,

$$\frac{dI_{LOAD}}{dt} = (V - R I_{LOAD}) \left(\frac{1}{L} \right) \quad (45)$$

Then, the load current at time t will be achieved by combining the two equations (44) and (45) as follows,

$$I_{LOAD}(t) = \frac{T_s}{L} (V(t) - R \times I_{LOAD}(t)) + I_{LOAD}(t - T_s) \quad (46)$$

Finally, by the shift of time at the load current from t to $(t+T_s)$, behavior of the load current in the future will be found in equation (47),

$$I_{LOAD}(t + T_s) = \{T_s \times V(t + T_s) + L \cdot I_{LOAD}(t)\} \left(\frac{1}{L + R \cdot T_s} \right) \quad (47)$$

In the equation (47), $V(t+T_s)$ represents the output voltage at $(t+T_s)$; this voltage is produced by appropriate control of the switches.

In the following, with an emphasis on the Fig.9, the predictive equations of future values will be displayed for inductor current (I_{L1}) in each of the three modes.

➤ Active State Operation

With the help of equations (37) and (43), the inductor current (I_{L1}) at time t will be achieved as follows,

$$I_{L1}(t) = \{T_s (V_i - V_{C1}(t)) + L_1 I_{L1}(t - T_s)\} \left(\frac{1}{L_1 + r \cdot T_s} \right) \quad (48)$$

And also, future behavior of equation (48) can be obtained with same as the shift of time as follows,

$$I_{L1}(t+T_s) = \left\{ T_s \left(V_i - \underbrace{V_{C1}(t+T_s)}_{\cong V_{C1}(t)} \right) + L_1 \cdot I_{L1}(t) \right\} \left(\frac{1}{L_1 + r \cdot T_s} \right) \quad (49)$$

Since the changes in the capacitor voltage is very low, so it can be concluded that $V_{C1}(t+T_s) \cong V_{C1}(t)$.

➤ Null State Operation

In this mode, the predictive equation for inductor current (I_{L1}) is similar to Active State Operation. Pay attention to the equation (50),

$$I_{L1}(t+T_s) = \left\{ T_s (V_i - V_{C1}(t+T_s)) + L_1 \cdot I_{L1}(t) \right\} \left(\frac{1}{L_1 + r \cdot T_s} \right) \quad (50)$$

Here, also, according to the above mentioned reason it can be assumed that $V_{C1}(t+T_s) \cong V_{C1}(t)$.

➤ Shoot-Through Operation

In this state, since the input voltage at the input quasi impedance-network (V_i) does not effect on the circuit, considering the Fig.9 and equations (41) and (43), the predictive equation for inductor current (I_{L1}) will be according to the following equation,

$$I_{L1}(t) = \left\{ T_s V_{C1}(t) + L_1 I_{L1}(t-T_s) \right\} \left(\frac{1}{L_1 + r \cdot T_s} \right) \quad (51)$$

The equation for predicting the inductor current is gained from the following formula,

$$I_{L1}(t+T_s) = \left\{ T_s \underbrace{V_{C1}(t+T_s)}_{\cong V_{C1}(t)} + L_1 \cdot I_{L1}(t) \right\} \left(\frac{1}{L_1 + r \cdot T_s} \right) \quad (52)$$

It is observed that in mentioned modes, another relevant variable to predict future behavior inverter was calculated.

Now, without any waste of time, capacitor voltage (V_{C1}) at the QZSI shall be calculated in three modes of operation. Therefore,

➤ Active State Operation

With the help of equations (36) and (42), the capacitor voltage (V_{C1}) at time t will be achieved as follows,

$$V_{C1}(t) = \frac{T_s}{C_1} (I_{L1}(t) - I_{INV}(t)) + V_{C1}(t-T_s) \quad (53)$$

$I_{INV} = I_{LOAD} \rightarrow$ in Active state

And also, future behavior of equation (53) can be obtained with same as the shift of time as follows,

$$V_{C1}(t+T_s) = \frac{T_s}{C_1} \left\{ I_{L1}(t+T_s) - \underbrace{I_{LOAD}(t+T_s)}_{\text{Equation (33)}} \right\} + V_{C1}(t) \quad (54)$$

➤ Null State Operation

By using equations (38) and (42), the capacitor voltage (V_{C1}) at time t will be achieved as follows,

$$V_{C1}(t) = \frac{T_s}{C_1} I_{L1}(t) + V_{C1}(t-T_s) \quad (55)$$

And its predictive equation will be as follows,

$$V_{C1}(t+T_s) = \frac{T_s}{C_1} I_{L1}(t+T_s) + V_{C1}(t) \quad (56)$$

➤ Shoot-Through Operation

By applying the equations (40) and (42), the capacitor voltage (V_{C1}) at time t will be achieved as follows,

$$V_{C1}(t) = \frac{-T_s}{C_1} I_{L1}(t) + V_{C1}(t-T_s) \quad (57)$$

And its predictive equation will be as follows,

$$V_{C1}(t+T_s) = \frac{-T_s}{C_1} I_{L1}(t+T_s) + V_{C1}(t) \quad (58)$$

In this way, all three required variables in order to study of behavior of the QZSI predictions were calculated for each of the three modes of operation.

B.v Predictive Control Scheme

In fact the predictive control strategy, proposed in this paper for the QZSI, is based on this principle that the future values of the load current (I_{LOAD}), the inductor current (I_{L1}), and capacitor voltage (V_{C1}) are predicted for the essential switching states produced by the inverter, by means of (47), (49), (52), (54), (56), and (58). In achieving this object, it is required to measure the present time of these variables. After acquiring the predictions, a cost function (CF) is evaluated for each switching state. Eventually, the switching state which minimizes the CF is chosen and applied during the next sampling time.

In this part, the cost function for the QZSI must be defined. Therefore, the requirements related to the variables control will be reviewed once again; as follows,

- The load current reference tracking
- The inductor current reference tracking
- The capacitor voltage reference tracking

As a result, this requirement should be exist in the cost function.

By defining the following errors,

$$\text{Er}I_{\text{LOAD}_{\text{Re}}}(t+T_s) = I_{\text{LOAD}_{\text{Re}}}^*(t+T_s) - I_{\text{LOAD}_{\text{Re}}}^{\text{P}}(t+T_s) \quad (59)$$

$$\text{Er}I_{\text{LOAD}_{\text{Im}}}(t+T_s) = I_{\text{LOAD}_{\text{Im}}}^*(t+T_s) - I_{\text{LOAD}_{\text{Im}}}^{\text{P}}(t+T_s) \quad (60)$$

$$\text{Er}V_{\text{C1}}(t+T_s) = V_{\text{C1}}^*(t+T_s) - V_{\text{C1}}^{\text{P}}(t+T_s) \quad (61)$$

$$\text{Er}I_{\text{L1}}(t+T_s) = I_{\text{L1}}^*(t+T_s) - I_{\text{L1}}^{\text{P}}(t+T_s) \quad (62)$$

Then, the cost function will be determined as follows so that this CF considers the absolute error between the reference values and the predicted values,

$$\text{CF} = \left| \text{Er}I_{\text{LOAD}_{\text{Re}}}(t+T_s) \right| + \left| \text{Er}I_{\text{LOAD}_{\text{Im}}}(t+T_s) \right| + \text{wf}_{V_{\text{C1}}} \left| \text{Er}V_{\text{C1}}(t+T_s) \right| + \text{wf}_{I_{\text{L1}}} \left| \text{Er}I_{\text{L1}}(t+T_s) \right| \quad (63)$$

In the above relations, symbol of 'Er' is the same error and symbol of '*' represents reference value of variables and as well, symbol of 'P' represents predicted value of variables. Also, it can be seen that the load current has both real (Re) and imaginary (Im) components. These two components are generated by the Clark and three-phase currents i.e. i_a , i_b , and i_c .

In relation (63) have been used two criteria to the relevance control objectives. These two criteria are called weighting factors namely ' $\text{wf}_{V_{\text{C1}}}$ ' and ' $\text{wf}_{I_{\text{L1}}}$ '. Although this parameter is a scalar it should be pointed out that the adjustment of 'wf' is still an open and interesting topic for study. Precise adjustment of the weighting factor is important because by using that can have a control system with favorable performance. For systems with a finite number of control actions, finite input sets, or state alphabet, one method to adjust the parameter is to simply evaluate the performance of specific system variables by simulations to determine the best value [29]. For cost functions with equally important terms, the cost function must be normalized, and then the weighting factor must be set to $\text{wf} = 1$. With this value the system will be controlled and, for fine

tuning, branch and bound can be used or slight variations of 'wf' around $\underline{1}$ can be tested [29]. In this paper $wf_{V_{Cl}} = 0.85$ and $wf_{I_{L1}} = 3.95$ is considered, of course, by trial and error.

The proposed predictive control scheme for the QZSI in the wind energy conversion system based on PMSG is shown in Fig.11.

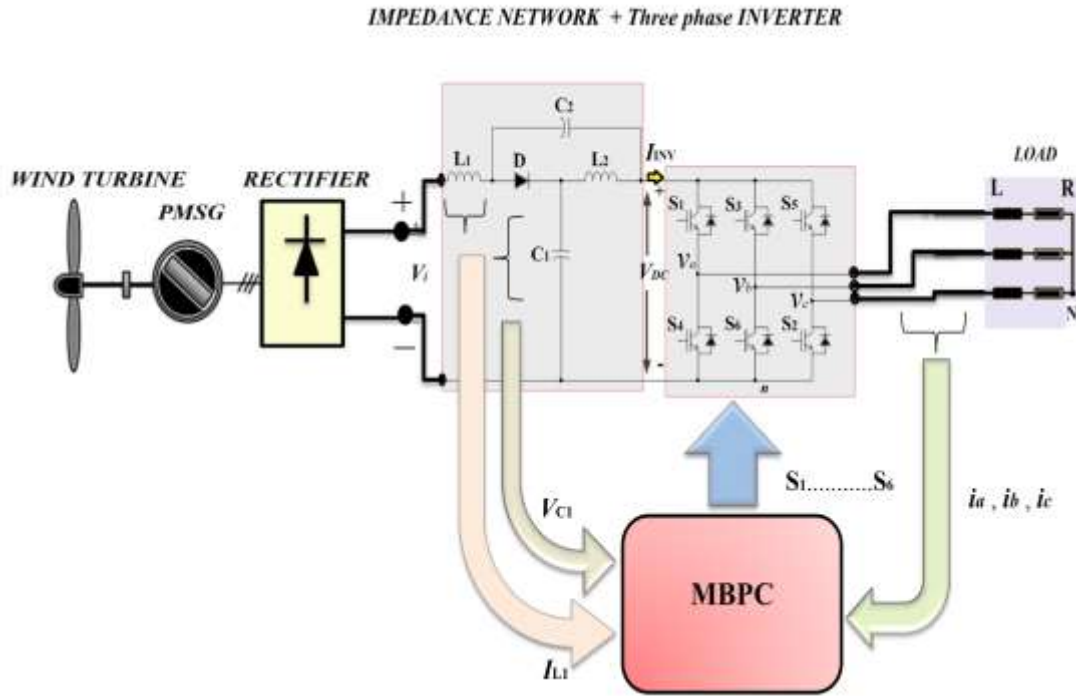


Figure.11. Scheme of the proposed predictive control strategy for QZSI

VIII. Simulation Results

To verify the performance of the proposed control strategy for both Quasi Impedance-Source Inverter (QZSI) and the rectifier associated with the PMSG in the wind turbine system, a series of simulation tests developed under MATLAB/Simulink software were carried out.

The fundamental simulation parameters have been given in Table 3. The accurate calculation of these parameters and their associated relationships is clearly shown in [30]. The sampling time in this control is $T_s = 25\mu s$. The intended switching frequency of proposed predictive control strategy is 10 kHz. It should be noted that there is no requirement for a modulator, which is the principal part of the traditional controller.

Table 3: Simulation parameters

R : load resistance	12 Ω
L : load inductance	12 mH
T_s : sampling time	25 μ s
QZSI inductance	350 μ H
QZSI capacitance	330 μ F
ω^* : speed reference of the PMSG	225 rad/s
Np : number of pole pairs for PMSG	4
I_{s-d}^* : stator current reference at d component	0
V_i : input voltage	55 v

At first, the response speed of the generator is shown in Fig.12. As seen in the figure, there is a step change in the speed at instant $t = 0.24$ sec. It is obvious that PMSG speed tracks their reference very well.

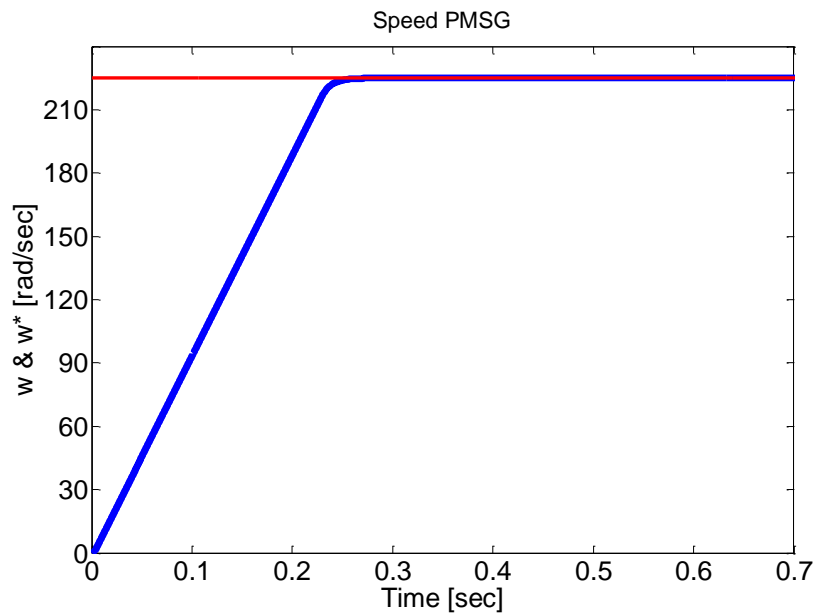


Figure.12. Tracking speed and its reference of PMSG

Assuming the wind speed is considered constant at all times, it is seen that speed of the generator is completely smooth. It is worth noting that wind speed in this paper is considered 13 m/sec. It can be said that due to the desirable design and implementation of the proposed predictive strategy on the rectifier associated with the PMSG, the accuracy of tracking speed is really high. In the following three-phase shown load current is shown in Fig.13. It is clear that this current is sine exactly.

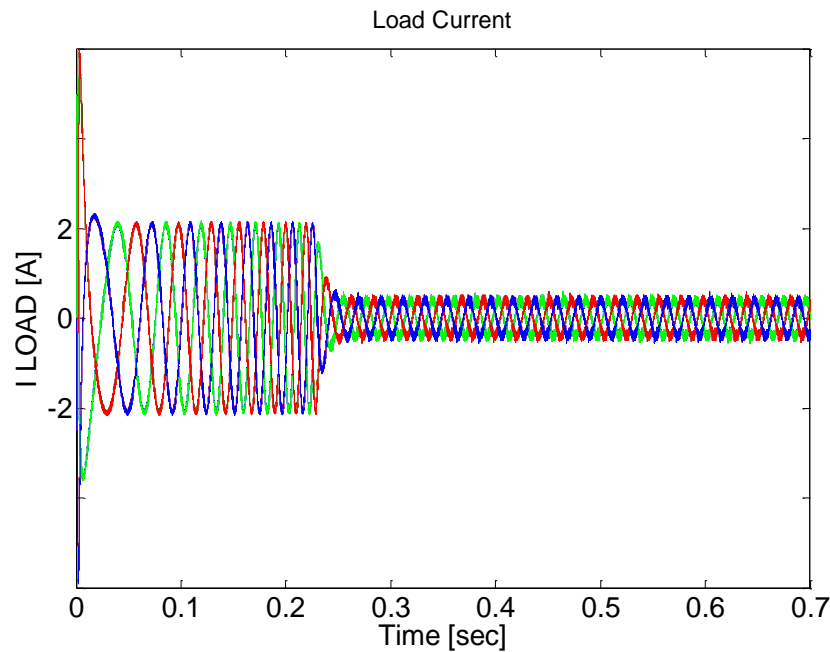


Figure.13. Tracking three-phase load current and its reference

As can be observed from the figure, the dynamics response of the current is quite fast. Three-phase current have reached to their maximum value without any overshoot. Three-phase current has a step change at instant $t = 0.24$ sec that this change is equivalent to the change in speed generator. In Fig.13, it is clear that the three-phase load current have very small ripple. If the sampling time is reduced, for example from $T_s = 25\mu s$ to the $T_s = 15\mu s$, the existing ripple can be decreased. However, it is seen that the dynamic response is precisely tracking the reference values; and this is because the proposed strategy on the QZSI side is designed efficiently.

If a frequency spectrum analysis or FFT was performed on one of the phases of the load current, it is observed that the Total Harmonic Distortion (THD) is 1.77%. Total Harmonic Distortion is a qualitative parameter and represents to what extent a signal or waveform is close to the sinusoidal waveform. THD value is expressed based on the percentage. Whatever THD be lower the sinusoidal waveform quality will be better. The current spectrum of the proposed MBPC strategy is specified in Fig.14 by discrete spectral lines. In spite of the fact that the switching frequency for the proposed predictive control is not constant, it does not have great variation.

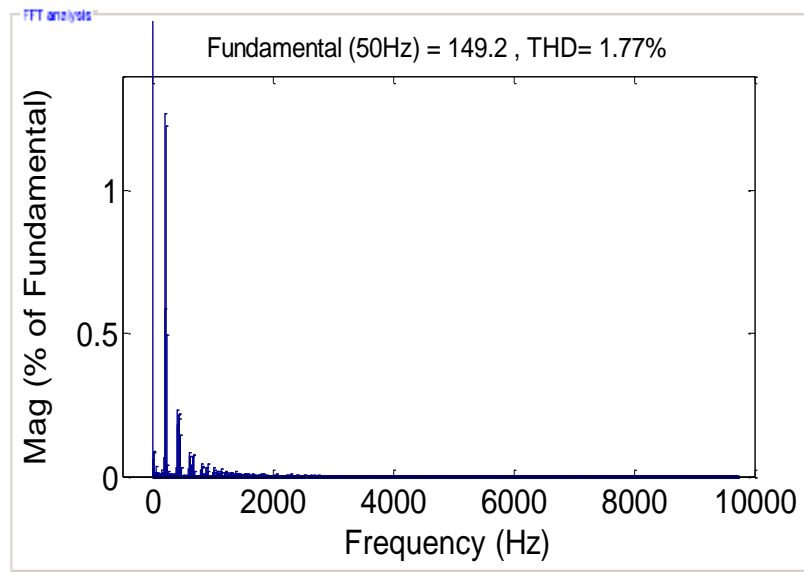


Figure.14. Load current spectrum analysis

In the following, the input current into the impedance network namely the inductor current (I_{L1}) is depicted in Fig.15. Inductor current corresponding to the three-phase load current has a step change at instant $t = 0.24$ sec. As can be seen from figure, this current has ripple; of course, the value of this ripple is very low. It is obvious that predicting the future values for the inductor current in the input impedance network carried out very well and these values accurately track their reference values.

It is known that tracking is highly robust because of the detailed design of the proposed MBPC strategy. Because of this strategy is robust should therefore state that this current tracking will be

there with its reference value despite the unbalanced grid; which of course we did not show this case in the paper.

The stator current of PMSG has been shown in the d & q components (I_{s-q} , and I_{s-d}) in Fig.16 and Fig.17, respectively. The stator current in q component has a step change at instant $t = 0.24$ sec, which PI controller available in Fig.6 responds to it. It can be seen from Fig.16, which the future values are predicted in the q component very well; and tracking the reference values has been done exactly.

It can be seen in Fig.17, which the stator current in d component is zero even during the transients due to acquire the maximum torque. Therefore, by using the proposed predictive control strategy has realized both terms available in the first cost function 'CF₁' namely stator current in the d & q components.

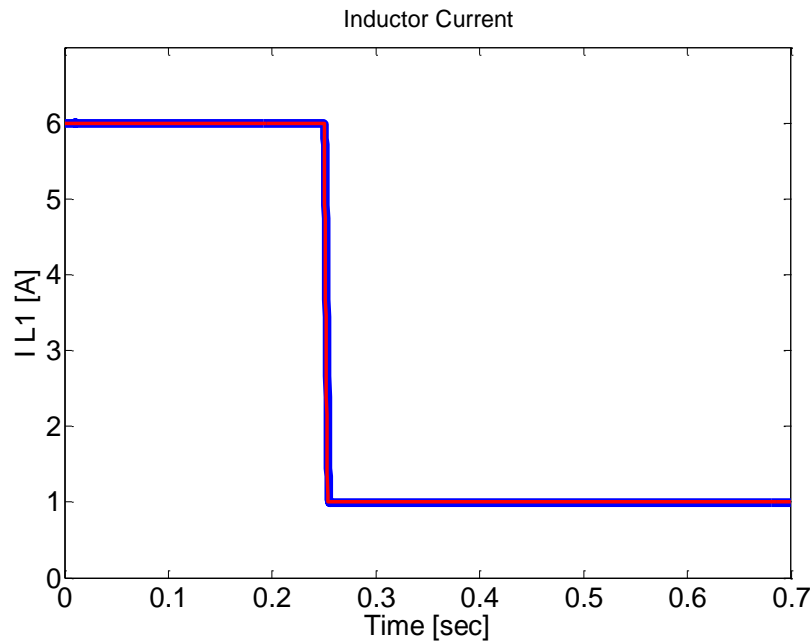


Figure.15. Tracking inductor current or input current into the impedance network along with its reference

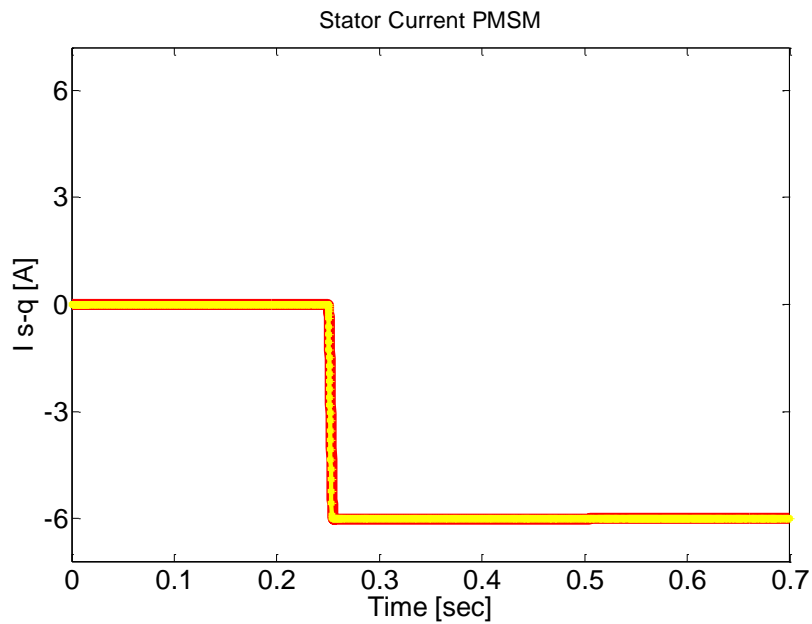


Figure.16. Tracking stator current of PMSG in q component and its reference

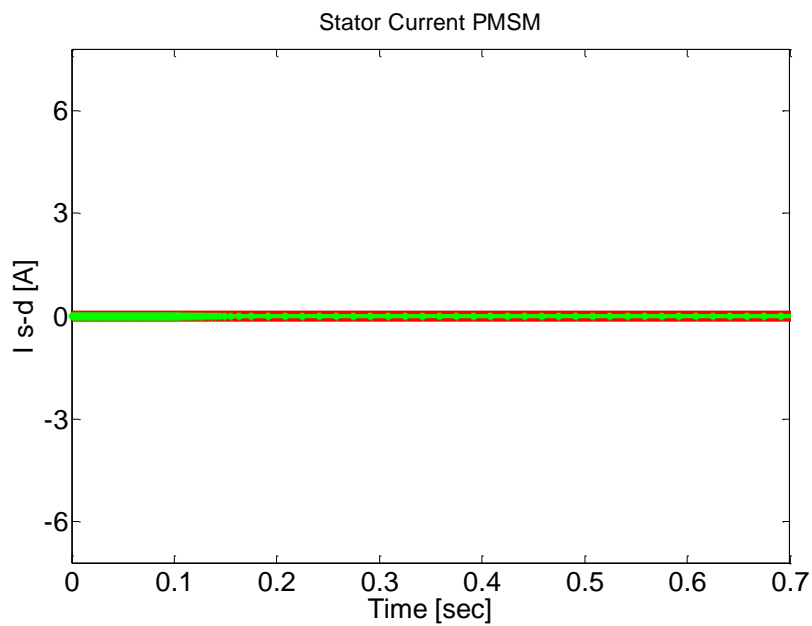


Figure.17. Tracking stator current of PMSG in d component and its reference

In the next phase of simulation results if the step change, applied to the previous results at instant $t = 0.24$ sec, be remove and as well as load inductance and load resistance changed from $R = 6 \Omega$ to $L = 6$ mH, then it should be noted that the three-phase load current and its reference are still sinusoidal but the existing ripple has been increased slightly. Of course, the ripple of current can be reduced by reducing sampling time which will lead to increased switching frequency.

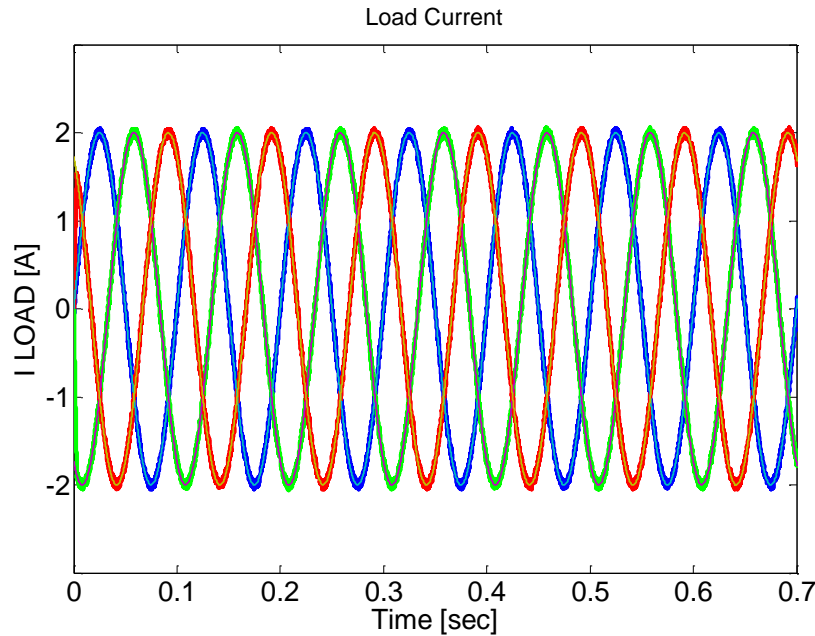
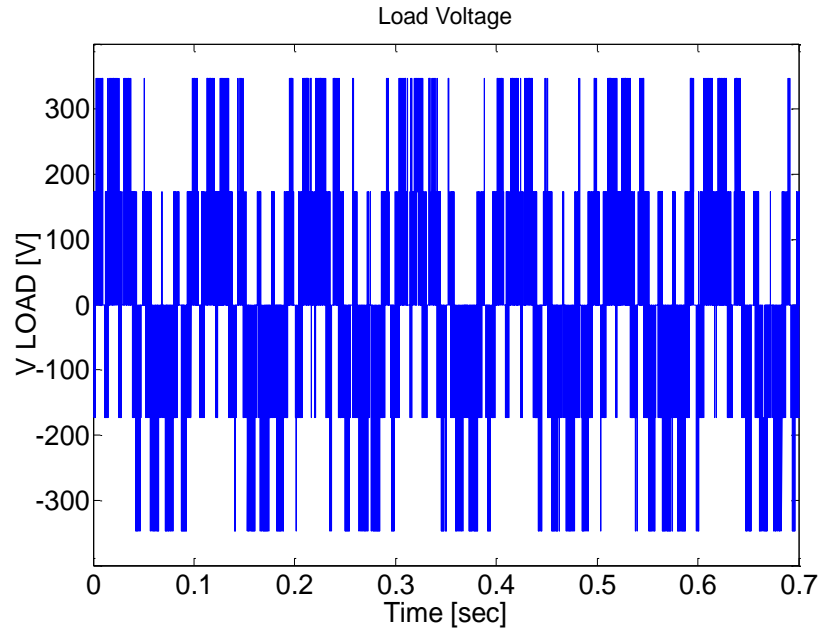


Figure.18. Tracking three-phase load current and its reference without the step change

It is known that like the previous case, the predicted values closely track the reference values. Therefore, we can conclude that the proposed MBPC strategy is certainly robust that even with the change of load parameters also does not lose its quality. The modified three-phase load current waveform is shown in Fig.18.

In Fig.19, the load voltage has been given in the phase a relative to the neutral point. It is worth mentioning that in obtaining this voltage is avoided from any kind of series-parallel or capacitive-inductive filter. It is clear that the switching action is desirable in the voltage because of the appropriate selection of sampling time.

Figure.19. Load voltage v_{an} without filter

Without any additional work, the response of the three-phase load voltage is depicted in Fig.22. But unlike the load voltage obtained in the previous case, here, a capacitive-inductive filter is used in order to obtain the load voltage in the output part. The value of parameters, used for filter, is $L_F = 4$ mH and $C_F = 25\mu\text{F}$.

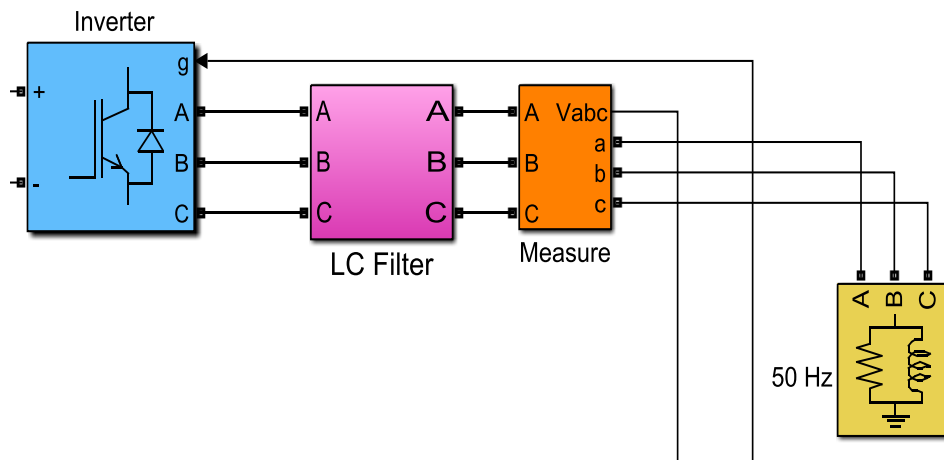


Figure.20. Filter circuit in output in the MATLAB/Simulink

How to connect and implementation of the output filter in MATLAB environment is depicted in Fig.20 and Fig.21.

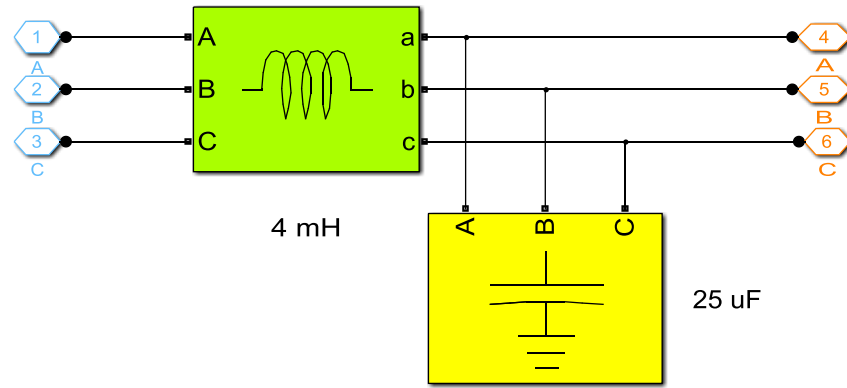


Figure.21. Value of parameters, used for filter, in the MATLAB/Simulink

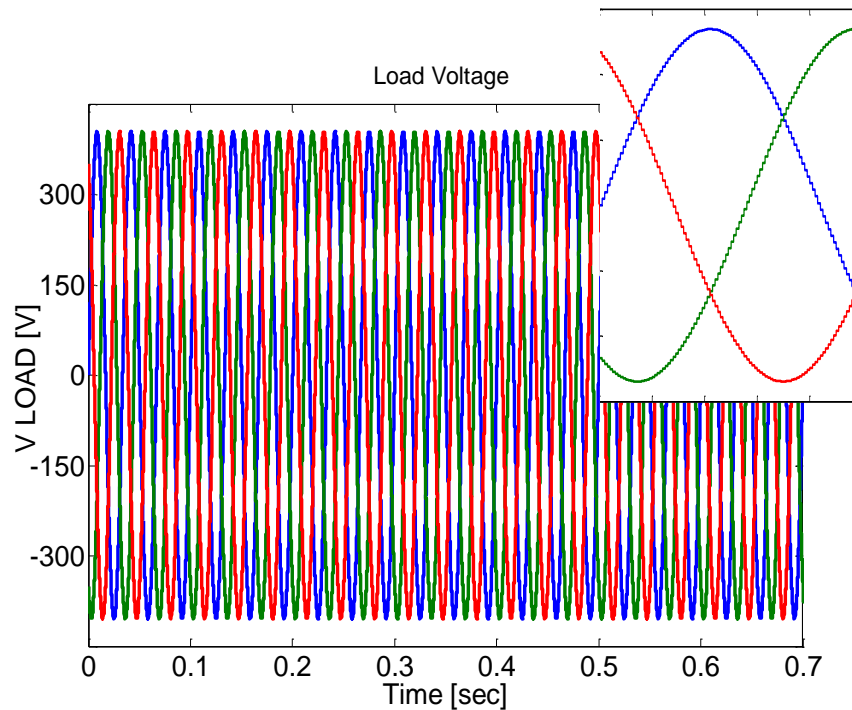


Figure.22. Load voltage with filter $L_F = 4 \text{ mH}$ and $C_F = 25 \mu\text{F}$

In Fig.22, if the load voltage has been expanded for example at timeframe 0.4 to 0.44 sec, then it is observed that this voltage would be quite sinusoidal. The load voltage like the load current has very small ripple. It is observed that due to the use of powerful predictive strategy, the dynamic response of voltage is fast. In fact, efficiency and effectiveness of the proposed predictive control strategy is completely evident.

In the following, the dynamic response of the first capacitor voltage (V_{C1}) in the impedance network is given in Fig.23. Although, the voltage faces with the little fluctuation around the reference value, it is obvious that the voltage is tracking the reference value very well. After a while the capacitor voltage starts from zero, in fact, it is being charged; then, it will be a constant value.

It is pointed out to this issue that the weighting factor which was previously defined in the cost function and its value was specified here shows its effectiveness.

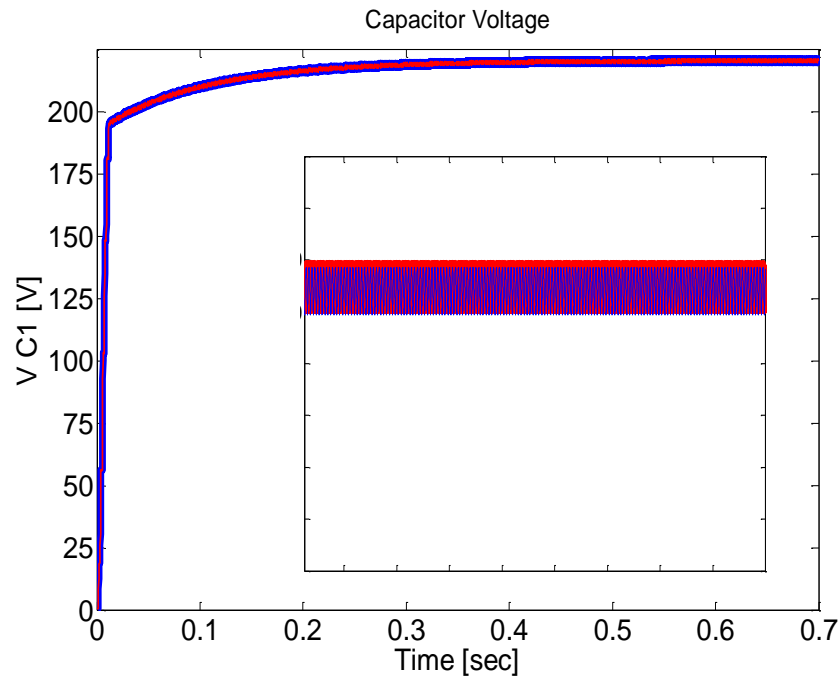


Figure.23. Tracking capacitor voltage (V_{C1}) and its reference in the impedance network

If this factor can't be accurately determined, then the corresponding strategy will lose its weight of control; consequence of this subject can be the emergence of noise, vibrations, and the lack of accurate tracking.

Also, in Fig.24 the second capacitor voltage (V_{C2}) in the impedance network is shown.

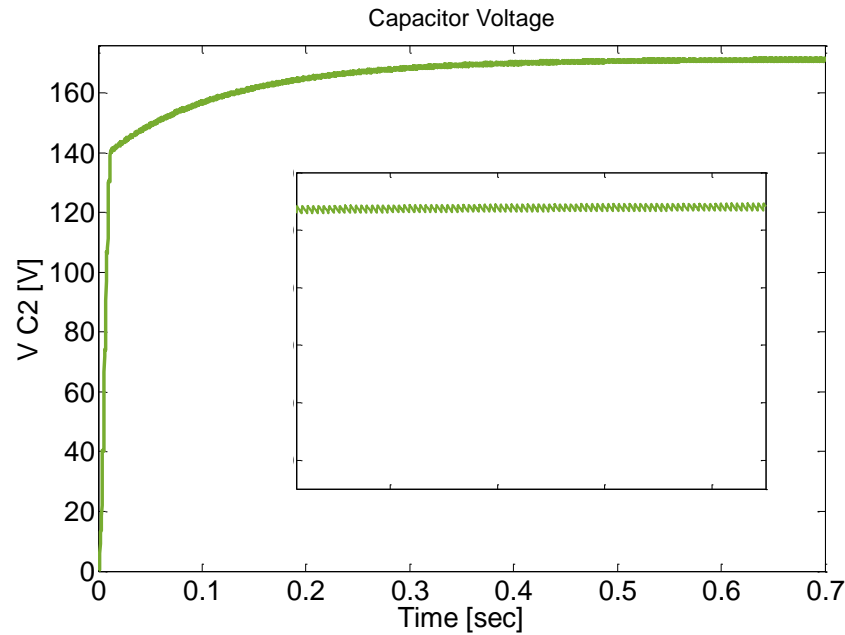
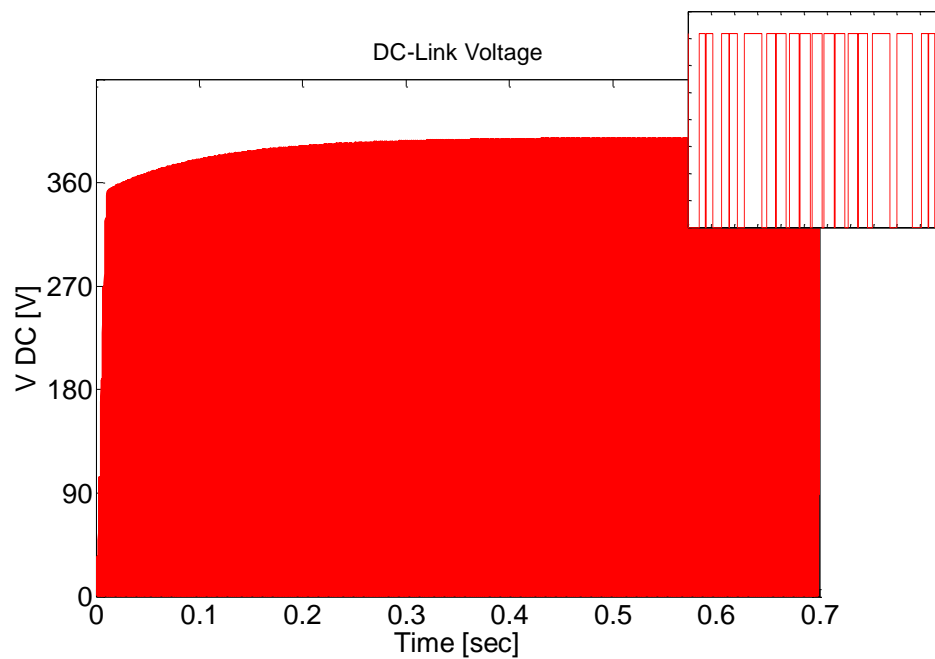
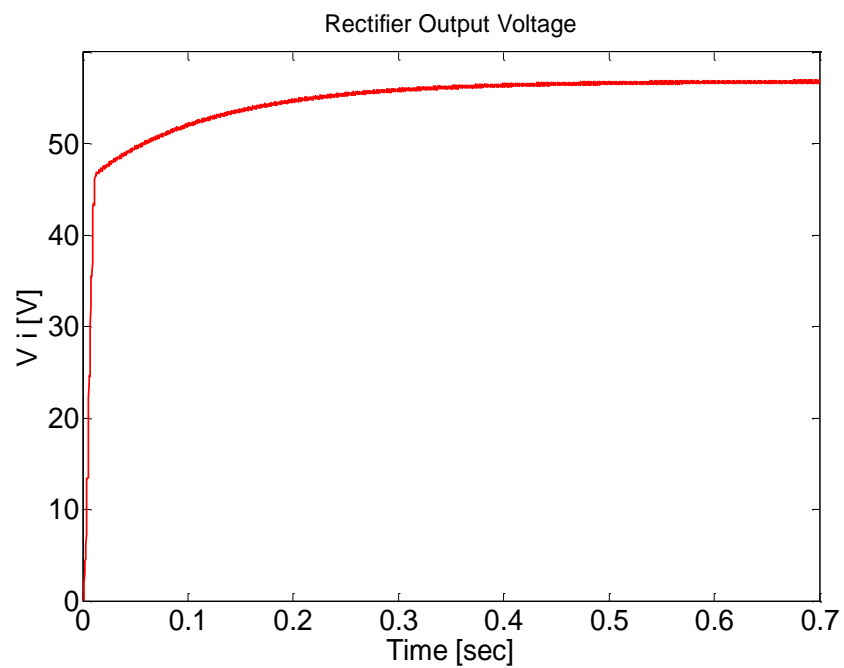


Figure.24. Capacitor voltage (V_{C2}) in the impedance network

The DC voltage (V_{DC}) or inverter voltage is depicted in Fig.25. In accordance with the inverter circuit, it is clear that the input voltage to the inverter is the sum of two capacitor voltages, i.e., V_{C1} and V_{C2} . The Inverter voltage is increased slowly and smoothly at wind speed 13 m/sec; then it reaches a constant value. This point is quite definite in figure which the DC voltage is devoid of any overshoot that this is benefits of proposed predictive control strategy. It can be expanded waveform in a particular period for example 0.4 to 0.4001 sec in order to better understand the DC signal.

Also, the input voltage (V_i) or voltage at the input quasi impedance-network is depicted in Fig.26. In accordance with the inverter circuit, it is clear that the voltage at the input quasi impedance-network is the subtraction of two capacitor voltages, i.e., V_{C1} and V_{C2} . In fact, this voltage is the same rectifier output voltage.

Figure.25. DC voltage (V_{DC}) or inverter voltageFigure.26. Input voltage (V_i) or rectifier output voltage

The implementation time for the control algorithm is about $12\mu\text{s}$. In Fig.28, three-phase load current is given. As can be seen the current is sine in practice. The current ripple is very small with low harmonic distortion. In the load current there is no overshoot. The amplitude of the reference load current has been set to 2 A in a frequency of 50 Hz. The behavior of the load voltage in one phase v_{an} at steady state operation has been depicted in Fig.29.

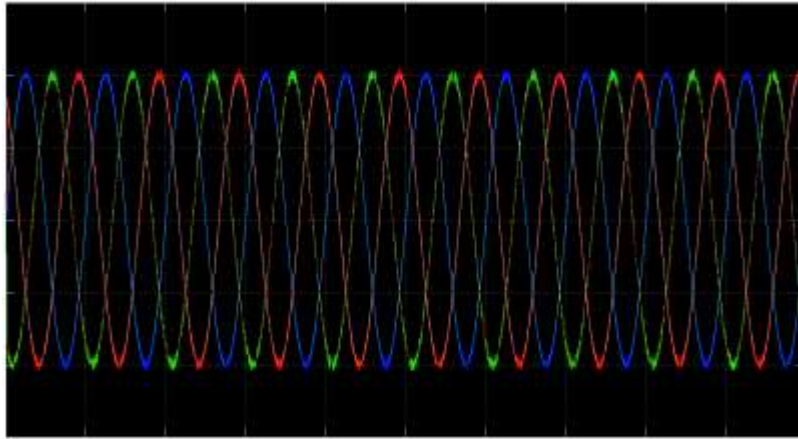


Figure.28. Experimental result for three-phase load current-(2 A/div)

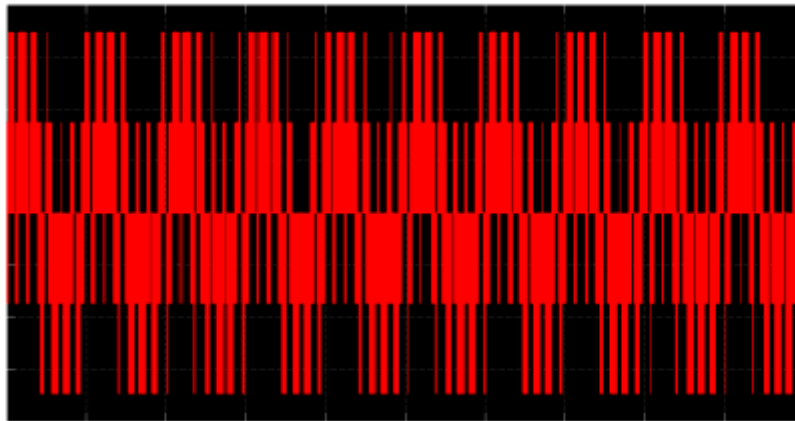


Figure.29. Experimental result in one phase v_{an} load voltage-(150 V/div)

X. Conclusion

In this paper, two predictive controller based on model was presented. The controllers, which take advantage from the predictive control strategy, have been implemented on a wind energy conversion system based on Permanent Magnet Synchronous Generator (PMSG). One of the proposed controllers is used to control the stator current in side of rectifier associated with the PMSG and the other is used to control the inductance current, capacitor voltage, and load current in side of three-phase Quasi Impedance-Source Inverter (QZSI). The use of this kind of inverter with the application of wind energy conversion system with the predictive control has not been used in any scientific papers. All of the mentioned control objectives were collected in two cost functions. At the end, the simulation results had been shown in two cases of software (MATLAB/Simulink) and experimental. The acquired results determined that the proposed predictive controllers can guarantee a constant capacitor voltage and sinusoidal three-phase load current with high dynamic performance. It is worth noting that the proposed predictive controller does not need any type of linear controller or modulation technique compared to the other control strategies. The responses of simulation showed robustness, effectiveness and efficiency of predictive control strategy and proposed controllers. The predictive control strategy and its applications in the industry fully have been shown in [23, 31- 34].

References

- [1] Y. Haile, K. Buse, C. Laszlo, R. Saillant and J. Gaskin, "Eco-communal management, transition engagement, and connectedness A moderated mediation model for the performance of renewable energy projects in emerging economies", International Conference on Renewable Energy Research and Applications (ICRERA), IEEE, 2015, pp. 683 - 688.
- [2] C. B. Mosleh, P. Rahme, P. Beaino, R. Mattar and E. A. Nassif, "Contribution to clean energy production using a novel wave energy converter: Renewable energy", Renewable Energies for Developing Countries (REDEC), 2014 International Conference on, IEEE, 2014, pp. 108 - 111.
- [3] J. C. Y. Hui, A. Bakhshai and P. K. Jain, "An Energy Management Scheme With Power Limit Capability and an Adaptive Maximum Power Point Tracking for Small Standalone PMSG Wind Energy Systems", IEEE Transactions on Power Electronics, vol. 31, No. 7, 2016, pp. 4861 - 4875.
- [4] R. A. Gupta, B. Singh and B. B. Jain, "Wind energy conversion system using PMSG", Recent Developments in Control, Automation and Power Engineering (RDCAPE), IEEE, 2015, pp. 199 - 203.

- [5] A. Rolán, F. C. López, S. Bogarra, L. Monjo and J. Pedra, "Reduced-Order Models of Squirrel-Cage Induction Generators for Fixed-Speed Wind Turbines Under Unbalanced Grid Conditions", *IEEE Transactions on Energy Conversion*, Vol. 31, No. 2, 2016, pp. 566 - 577.
- [6] M. H. Zamani, S. H. Fathi, G. H. Riahy, M. Abedi and N. Abdolghani, "Improving Transient Stability of Grid-Connected Squirrel-Cage Induction Generators by Plugging Mode Operation", *IEEE Transactions on Energy Conversion*, Vol. 27, No. 3, 2012, pp. 707 - 714.
- [7] R. Joseph and L. Umanand, "A Brushless Wound Rotor Induction Generator for Variable Speed Microhydel Plants Without Ballast Load", *IEEE Transactions on Sustainable Energy*, Vol. 6, No. 1, 2015, pp. 20 - 27.
- [8] Z. Li and J. Ma, "Research on variable-speed and variable-pitch wind doubly fed induction generator system and its multivariable coordinated control", *The 27th Chinese Control and Decision Conference (2015 CCDC)*, IEEE, 2015, pp. 5865 - 5869.
- [9] A. S. Helmy, A. Shaltout and N. Abdel-Rahim, "Improving the efficiency of a Doubly-Fed Induction Generator in variable speed wind turbines under different modes of operation considering core loss", *Smart Energy Grid Engineering (SEGE)*, IEEE, 2015, pp. 1 - 8.
- [10] N. Budisan, R. Boraci, C. Koch-Ciobotaru, G. Prostean and C. Musca, "On permanent-magnet synchronous generator current harmonics, due to rectifier at the generator end of the variable speed generator sets converter systems", *Computational Cybernetics and Technical Informatics (ICCC-CONTI)*, IEEE, 2010, pp. 471 - 474.
- [11] F. Blaabjerg and K. Maand, "Future on Power Electronics for Wind Turbine Systems", *IEEE Journal of Emerging and Selected Topics in Power Electronics*, Vol. 1, No. 3, 2013, pp. 139 - 152.
- [12] L. H. Hansen, P. H. Madsen, F. Blaabjerg, H. C. Christensen, U. Lindhard and K. Eskildsen, "Generators and power electronics technology for wind turbines", *Industrial Electronics Society IECON '01. The 27th Annual Conference of the IEEE*, 2001, pp. 2000 - 2005.
- [13] Z. Chen, J. M. Guerrero and F. Blaabjerg, "A Review of the State of the Art of Power Electronics for Wind Turbines", *IEEE Transactions on Power Electronics*, Vol. 24, No. 8, 2009, pp. 1859 - 1875.
- [14] H. S. Kim and D. Dah-Chuan Lu, "Review on wind turbine generators and power electronic converters with the grid-connection issues", *Universities Power Engineering Conference (AUPEC). 20th Australasian*, IEEE, 2010, pp. 2000 - 2005.
- [15] C. N. Wang, X. K. Le and W. C. Lin, "Modeling and Simulation of Autonomous Control PMSG Wind Turbine", *Computer, Consumer and Control (IS3C)*, IEEE, 2014, pp. 1144 - 1147.
- [16] V. Z. Manusov and S. K. Khaldarov, "Adaptive control of a variable wind speed turbine based on fuzzy logic", *Actual Problems of Electronics Instrument Engineering (APEIE)*, IEEE, 2014, pp. 829 - 831.
- [17] L. Qingsong and Q. Suxiang, "Sliding mode variable pitch control of wind turbine via fuzzy neural network", *Control Conference (CCC). 31st Chinese*, IEEE, pp. 3187 - 3191.
- [18] X. Zhang, W. Wang, D. Liu, H. Wang, X. Cao and S. He, "Matrix converter control study of doubly-fed induction wind turbine generator system", *11th International Conference on Power Electronics and Drive Systems*, IEEE, 2015, pp. 139 - 142.
- [19] Z. Zhang and R. Kennel, "Direct Model Predictive Control of three-level NPC back-to-back power converter PMSG wind turbine systems under unbalanced grid", *International Symposium on Predictive Control of Electrical Drives and Power Electronics (PRECEDE)*, IEEE, 2015, pp. 97 - 102.

- [20] Z. Zhang, Y. Zhao, W. Qiao and L. Qu, "A Discrete-Time Direct Torque Control for Direct-Drive PMSG-Based Wind Energy Conversion Systems", IEEE Transactions on Industry Applications, Vol. 51, No. 4, 2015, pp. 3504 - 3514.
- [21] F. Louar, A. Ouari, A. Omeiri, F. Senani and A. Rahab, "Direct power control (DPC) of PMSG based wind energy conversion system", 2015 4th International Conference on Electrical Engineering (ICEE), IEEE, 2015, pp. 1 - 6.
- [22] A. Hussien, M. Taha and Ossama A. Mahgoub, "Design and Control of a Quasi-Z-Source Inverter Based for Wind Power Generation using PMSG", Environment and Electrical Engineering (EEEIC), IEEE, 2015, pp. 2050 - 2055.
- [23] H. Javaheri Fard, H. R. Najafi and H. Eliasi, "Active and reactive power control via currents of a rotor's d and q components with nonlinear predictive control strategy in a doubly fed induction generator based on wind power system", Energy Equipment and Systems, Vol. 3, No. 2, 2015, pp. 143 - 157.
- [24] Y. Liu, H. Abu-Rub, B. Ge, F. Blaabjerg, O. Ellabban and P. C. Loh, "Impedance Source Power Electronic Converters", September 2016, Wiley-IEEE Press.
- [25] O. Ellabban and H. Abu-Rub, "Z-Source Inverter: Topology Improvements Review", IEEE Industrial Electronics Magazine, Vol. 10, No. 1, 2016, pp. 6 - 24.
- [26] J. Anderson and F. Z. Peng, "A Class of Quasi-Z-Source Inverters", Industry Applications Society Annual Meeting, IEEE, 2008, pp. 1 - 7.
- [27] J. Anderson and F. Z. Peng, "Four quasi-Z-Source inverters", Power Electronics Specialists Conference, IEEE, 2008, pp. 2743 - 2749.
- [28] O. Ellabban, M. Mosa, H. Abu-Rub and J. Rodriguez, "Model Predictive Control of Grid Connected Quasi-Z-Source Inverter", Industrial Technology (ICIT), IEEE, 2013, pp. 1591 - 1596.
- [29] J. Rodriguez and P. Cortes, "Predictive Control of Power Converters and Electrical Drives", April 2012, Wiley-IEEE Press.
- [30] C. J. Gajanayake, D. M. Vilathgamuwa, and P. C. Loh, "Development of a Comprehensive Model and a Multi-loop Controller for Z-Source Inverter DG Systems", IEEE Transactions on Industrial Electronics, Vol. 54, No. 4, 2007, pp. 2352 - 2359.
- [31] H. Javaheri Fard, H.R. Najafi and G. Heidari, "Design of Discrete Predictive Direct Power Control Strategy on the Doubly-Fed Induction Generator Based on Micro-Hydro Power Plant With the Aim of Active and Reactive Powers Control", 21st Conference on Electrical Power Distribution Networks Conference (EPDC), IEEE, 2016, pp. 118 - 124.
- [32] H. Javaheri Fard, H. R. Najafi and H. Eliasi, "Novel design and simulation of predictive power controller for a doubly-fed induction generator using rotor current in a micro-hydropower plant", Energy Equipment and Systems, Vol. 5, No. 1, 2017, pp. 43 - 58.
- [33] H. Javaheri Fard, H.R. Najafi and H. Eliasi, "Design and Implementation of the Predictive Current Control Strategy in the Form of Laboratory on Single Phase Photovoltaic Grid-Connected Inverter Based on Microcontroller Tms320lf2407a", 30th International Power System Conference (PSC), 2015, pp. 1 - 7.
- [34] M. Ramzi and H. Youlal, "Centralized Discrete State Space Model Predictive Control and Decentralized Pi-D Controller of an Aero thermic Process", S2IS Journal, Vol. 7, No. 4, 2014, pp. 1830 - 1849.